# Modeling functional piezoelectricity in perovskite superlattices with competing instabilities

Charles W. Swartz[1] and Xifan Wu[1,2,3,*]

[1]*Department of Physics, Temple University, Philadelphia, Pennsylvania 19122, USA*

[2]*Temple Materials Institute, Temple University, Philadelphia, Pennsylvania 19122, USA*

[3]*Institute for Computational Molecular Science, Temple University, Philadelphia, Pennsylvania 19122, USA*

(Received 21 September 2011; revised manuscript received 13 December 2011; published 2 February 2012)

Based on the locality principle of insulating superlattices, we apply the method of Wu *et al.* [Phys. Rev. Lett. **101**, 087601 (2008)] to the piezoelectric strains of individual layers under a fixed displacement field. For a superlattice of arbitrary stacking sequence, an accurate model is acquired for predicting piezoelectricity. By applying the model in the superlattices where ferroelectric and antiferrodistortive modes are in competition, functional piezoelectricity can be achieved. A strong nonlinear effect is observed and can be further engineered in the $PbTiO_3/SrTiO_3$ superlattice, and an interface enhancement of piezoelectricity is found in the $BaTiO_3/CaTiO_3$ superlattice.

DOI: 10.1103/PhysRevB.85.054102 PACS number(s): 77.22.Ej, 77.80.−e, 77.84.Lf

## I. INTRODUCTION

Multicomponent $ABO_3$ perovskite superlattices (SL's) provide a very promising way to design novel materials with multifunctional properties for device application.[1,2] Bridged by interfaces, distinct instabilities belonging to individual bulk constituents are in strong competition within these artificial materials. Functional properties such as polarization,[1–5] piezoelectric,[6,7] magnetoelectric,[8–10] and dielectric responses are found to be highly sensitive to interactive instabilities, sometimes resulting in unexpected enhanced functionalities.

Paraelectric (PE)/ferroelectric (FE) SL's with both antiferrodistortive (AFD) and FE instabilities have attracted intense interest recently.[2,4,11] The zone-boundary nonpolar AFD mode associated with oxygen octahedral rotation and the zone-center polar FE mode are usually found to be exclusive to each other in bulk perovskite. However, in SL's of $PbTiO_3$(PT)/$SrTiO_3$(ST) and $BaTiO_3$(PT)/$CaTiO_3$(ST), first-principles calculations revealed that the AFD and FE can coexist with an interface reconstruction.[2,4] In both cases, the competing AFD and FE modes at interfaces are predicted to enhance the polarization, which is consistent with the experimental observation.[2,12]

Clearly, for these insulating PE/FE SL's, both ionic and electronic interface effects should be well localized. The local electrostatic property will only be different from the bulk material within a few layers away from the interface under the fixed displacement field. Thus the interface dipoles can be accurately described by a truncated cluster expansion (TCE) model developed by Wu *et al.*,[13] in which the electronic states of the interfaces are represented by the maximally localized Wannier functions through a unitary transformation from Bloch-like orbitals.[14–16] Based on the above, SL design can be performed in the AFD/FE competing system, where the interface is expected to increase the overall FE. For quite some time, the focus was to explore the functional polarization.[2–4,17–19] Piezoelectricity,[20–23] another important functionality, describes the coupling between polarization and strain. Its interface mechanism and SL design rule have not yet been addressed in these intriguing systems with competing instabilities.

In this paper, we show that functional piezoelectricity can be designed in the SL's through the AFD and FE competition and its electric-field dependence. We further apply our TCE model to the piezoelectric strain of the SL's in a fixed displacement field. In combination with a similar treatment of Wannier-based layer polarization, we arrive at an accurate modeling for predicting the piezoelectric tensor for an arbitrary sequence of SL's. In bulk ST, we discover a strong nonlinear piezoelectric response originating from the completely suppressed AFD in a large applied electric field. We use the model to demonstrate that the electric field of this nonlinear piezoelectricity can be reduced to a much smaller magnitude with a largely increased field tunability by changing the PT fraction in PT/ST SL's. With this model, we are able to systematically study the interface effect on the piezoelectric response in both BT/CT and PT/ST SL's. In BT/CT SL's, we find a novel interface enhancement of piezoelectricity.

## II. METHODOLOGY AND CALCULATIONS

The first-principles calculations are carried out in two series of SL's $n$PT/$m$ST and $n$BT/$m$CT with both AFD and FE instabilities. These include the bulk PT, ST, BT, CT, and all period-4 SL's ($n + m = 4$) stacked in the [001] direction. The fixed in-plane lattice constant is chosen as $a_0 = 7.275$ bohr, the computed equilibrium lattice constant for bulk cubic $SrTiO_3$. We assume the epitaxial growth of the SL's on $SrTiO_3$, which is consistent with the recent experiments.[2,6] Both the FE mode along [001] and the AFD mode associated with oxygen octahedral $TiO_6$ rotation around the [001] axis have been explicitly included in the sublattice structure of $P4bm$ space-group symmetry. To this end, a 40-atom tetragonal supercell is adopted with lattice vectors of length $\sqrt{2}a_0$ in the [110] and [1$\bar{1}$0] directions and [1$\bar{1}$0] directions and $c \approx 4a_0$ along the [001] direction. We neglect the nanodomain formation,[24] which might be important for these systems.

We use density-functional theory implemented in the LAUTREC code package[25] to perform structural relaxations (including both force and stress relaxations) and electron minimizations at fixed electric displacement fields. The local-density approximation[26] is adopted and plane-wave calculations are implemented in the projector augmented-wave

 ©2012 American Physical Society

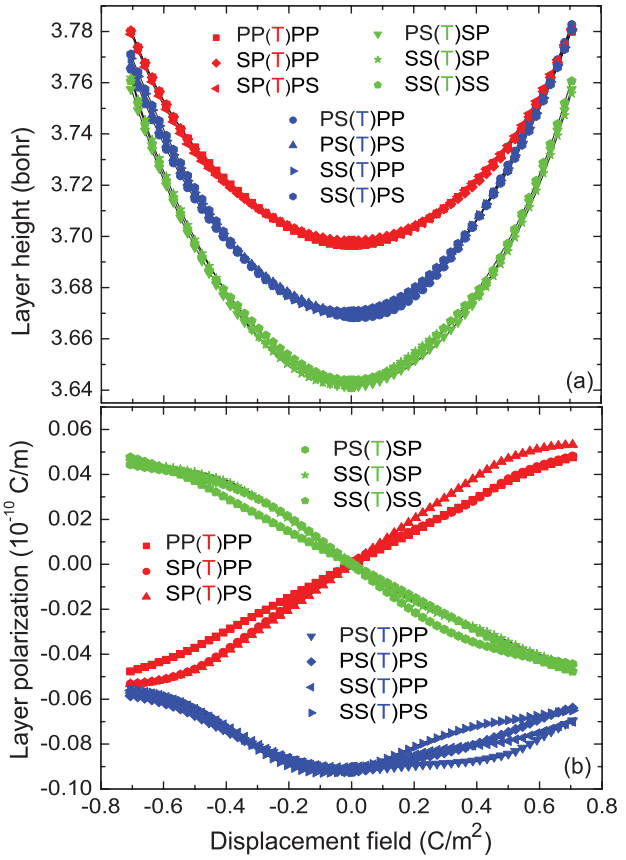


FIG. 1. (Color online) Dependence of $TiO_2$(T) (a) layer height and (b) layer polarization (relative to the average of the $TiO_2$ planes of bulk $PbTiO_3$ and $SrTiO_3$) on chemical environment in PT/ST SL's [e.g., PS(T)SP denotes the layer height or layer polarization for a $TiO_2$ layer with two ST and two PT as its first and second nearest neighbors, respectively, in the superlattices]. Symbols represent direct DFT calculations, solid lines represent model predications. See the main text for more details.

framework.[27] We used a plane-wave cutoff energy of 80 Ry and a $4 \times 4 \times 1$ Monkhorst-Pack $k$ mesh.

Our model for piezoelectricity starts from the decomposition of the SL's into $AO$ and $BO_2$ layers along the [001] direction. For each fixed $D$-field point, both Wannier-based layer polarization $p_i(D)$ (Ref. 16) and the layer height $h_i(D)$ (Refs. 4 and 28) [which is directly related to piezoelectric strain $\eta_i(D)$] of each individual layer are computed from the relaxed electronic and ionic structure, respectively. Working with the constrained-$D$ field framework,[25] we employ the longitudinal boundary condition, which limits the force constant matrix to short-range interaction of a few neighbors.

In Fig. 1, we present the representative plots (symbols) for $h_j(D)$ and $p_j(D)$ in PT/ST SL's, obtained from direct decomposition of our first-principles results. As expected, the locality principle is satisfied not only on the layer polarization[13] but also the layer height. As a result, both $h_j(D)$ and $p_j(D)$ curves separate into clusters depending on the nearest-neighbor chemical environment. In can be seen that $p_j(D)$ is mostly determined by the identity of nearest neighbors and has a much weaker dependence on the second neighbors. Compared with $p_j(D)$, $h_j(D)$ shows a similar behavior with an even stronger localization. A clear local inversion symmetry breaking is also present in $h_j(D)$ as well as $p_j(D)$. As an example, the inversion symmetry breaking introduced by the first neighbors has a large asymmetric behavior for the $h_j(D)$ of $TiO_2$ in the middle of the S(T)P sequence. This asymmetric behavior becomes much weaker when the local inversion symmetry breaking occurs only on the second neighboring layers in SS(T)SP. In previous work,[13] it has been shown that a TCE model accurately captures the dependence of $p_i(D)$ on its local compositional environments. The similar locality of $h_i(D)$ indicates that $h_j(D)$ [as well as $p_j(D)$] can be accurately described by the TSE as

$$h_l(\{s\}) = J_0 + \sum_i \left(J_{l,i} s_i + J'_{l,i} s_i^2\right) + \sum_{ij} \left(J_{l,ij} s_i s_j + J'_{l,ij} s_i s_j^2 + J''_{l,ij} s_i^2 s_j^2\right) + \sum_{ijk} J_{l,ijk} s_i s_j s_k + \cdots . \quad (1)$$

The $D$-dependent $J$ terms are the effective cluster interaction coefficients (ECI's) and are computed from a database of $p_j(D)$ and $h_j(D)$ that have been determined from the first-principles results. The "pseudospin" variable is defined as $s_i = 1,0$ and is used to identity the $i$th $AO$ layer as either PbO(BaO) or SrO(CaO), respectively. Our TCE model will include the cluster interaction of one particular layer with the neighboring layers, up to second nearest neighbors, and interaction terms up to two body. As a result, all the truncated cluster terms are effectively included in the compositional environment of the period-4 SL's. The expressions for $h_{AO}$, $h_{TiO_2}$, $p_{AO}$, and $p_{TiO_2}$ with all the fitted ECI's will be given in the supplemental material.[29] The total supercell lattice constant is obtained from the sum of all the individual layer heights as $h(D) = \sum_i h_i(D)$ and the piezoelectric strain of the SL can be calculated by $\eta(D) = [h(D) - h(D=0)]/h(D=0)$. The electric equation of state of $\eta$ as a function of electric field $\mathcal{E}(D)$ will be obtained by numerical inversion. The electric field is computed by $\mathcal{E}(P) = D(P) - 4\pi P$, where the total polarization of the SL is given by $P(D) = h(D)^{-1} \sum_j p_j(D)$. It is then straightforward to compute the piezoelectric coefficient $d_{33} = \partial \eta_{33}/\partial \mathcal{E}$.

The computed curves for the model results of $p_j(D)$ and $h_j(D)$ in the PT/ST SL's are plotted (as solid lines) in Fig. 1. We can see that the quality of the fit is excellent, having an average rms error of $1.59 \times 10^{-14}$ C/m and $1.94 \times 10^{-4}$ bohr for the $p_j(D)$ and $h_j(D)$, respectively, in PT/ST and $1.60 \times 10^{-14}$ C/m and $3.93 \times 10^{-4}$ bohr, respectively, in BT/CT. A second confirmation comparing the total lattice height from direct first-principles results and the total lattice height calculated by our model is also contained in the supplemental material.[29]

Here we want to stress that the modeling of the individual layer height $h_j(D)$, instead of the total height $h(D)$ of the SL, is important for a more accurate piezoelectric model due the fact that the constituent layers each contribute differently to the total lattice height in conjunction with piezoelectricity's definition as the derivative of the strain with respect to the electric field. This derivative will obviously be sensitive to the accuracy of the strain model. We observed piezoelectric

average rms errors of 0.118 69 and 0.839 43 pm/V for BT/CT and PT/ST, respectively, using our layer height model as compared to errors of 0.5724 and 1.15587 pm/V using a similar model based on total lattice height.[13] A breakdown of the rms errors for each of the SL's is shown in the supplemental material,[29] where it can be observed that the previous model has deficiencies in describing nonbulk SL's. Furthermore, it is also important to stress that due to the short-range, layer-by-layer nature of our truncated TCE, the models of $p_j(D)$ and $h_j(D)$ can be naturally used to predict and design piezoelectricity of superlattices at the layer level. This enables us to study the piezoelectricity resulting from the AFD/FE competition under an applied electric field or at the interfaces systematically.

## III. RESULTS AND DISCUSSION

### A. Piezoelectricity under applied electric fields

It is well established that AFD and FE will compete with each other in bulk $ABO_3$.[11,30,31] Under an applied electric field, the FE will be strengthened by the coupling between the electric field and the polar mode, and the SL will be further polarized along the field direction. It is therefore expected that AFD will be suppressed with increased electric field. Indeed, in Fig. 2 we can see that the octahedral rotation is largely suppressed with increased $D$ magnitude in both bulk ST and strained bulk PT. Surprisingly, at $D \sim 0.4$ C/m$^2$ and $D \sim 0.6$ C/m$^2$, the octahedral rotation will be completely suppressed, resulting in a FE-only phase. At ground state, the bulk ST has an octahedral rotation of 5.8°. This is consistent with the previous reported LDA result by Sai and Vanderbilt (5.5°),[32] which is larger than the zero-temperature experimental value of 2.1°.[33] This large overestimation has been found to be due to the underestimated theoretical lattice constant by the LDA, which tends to overestimate the AFD instability. It is also important to notice that the $TiO_6$ rotation in bulk PT is *hidden* and cannot be observed experimentally. This is because the AFD instability is completely suppressed in the metastable region before the spontaneous polarization is reached ($D \simeq P = 0.8$ C/m$^2$). In the PT/ST SL's, the spontaneous polarization will be reduced and the AFD rotation will be recovered in the PT fraction. In contrast, octahedral rotations in strained bulk CT have a much weaker field dependence. The $TiO_6$ rotation in CT is only slightly decreased from 13° at $D = 0$, as shown in the inset of Fig. 2.[4] This is consistent with the much stronger AFD than FE instability, which results in the PE ground state for bulk CT. On the other hand, BT shows no AFD rotation at all for the whole field range. This is expected from the fact that bulk BT strongly resists AFD rotation with a robust FE ground state.

Since ST is PE at ground state, the disappearance of the AFD instability is experimentally measurable (located in the stable region of double-well potential) and indicates a physical phase transition driven by an applied electric field. As a signature, one can clearly see an additional peak of $d_{33}(\mathcal{E})$ in bulk ST in Fig. 3(a). However, it occurs at a very high electric field (centered around 600 MV/m). This is probably the reason why this phase transition has not been addressed yet in the literature. The $d_{33}(\mathcal{E})$ coefficient can be further decomposed into the product of piezoelectric $g$ tensor[21] and dielectric constant $\epsilon$ as $d_{33}(\mathcal{E}) = g_{33}\epsilon_{33}$,[21] where $g_{33} = \partial\eta_{33}/\partial D$ and $\epsilon_{33} = \partial\mathcal{E}/\partial D$.[21] In the dielectric constant $\epsilon$ of bulk ST, we identify a similar peak as shown in Fig. 3(b),

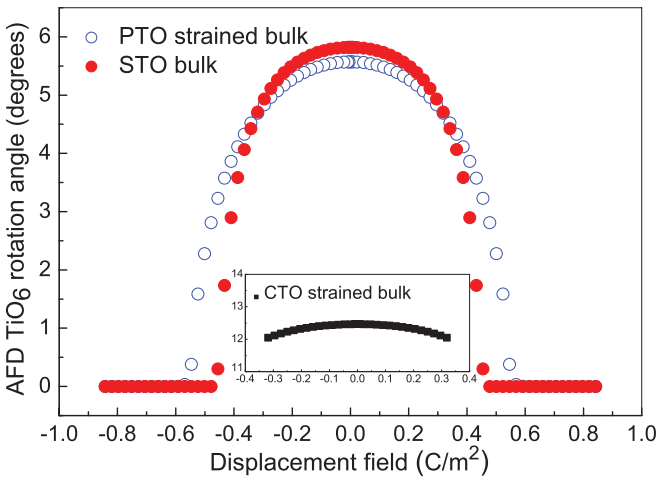


FIG. 2. (Color online) $TiO_6$ rotation as a function of the $D$ field for $TiO_6$ octahedral in bulk ST, strained bulk PT, and strained bulk CT (shown in the inset).

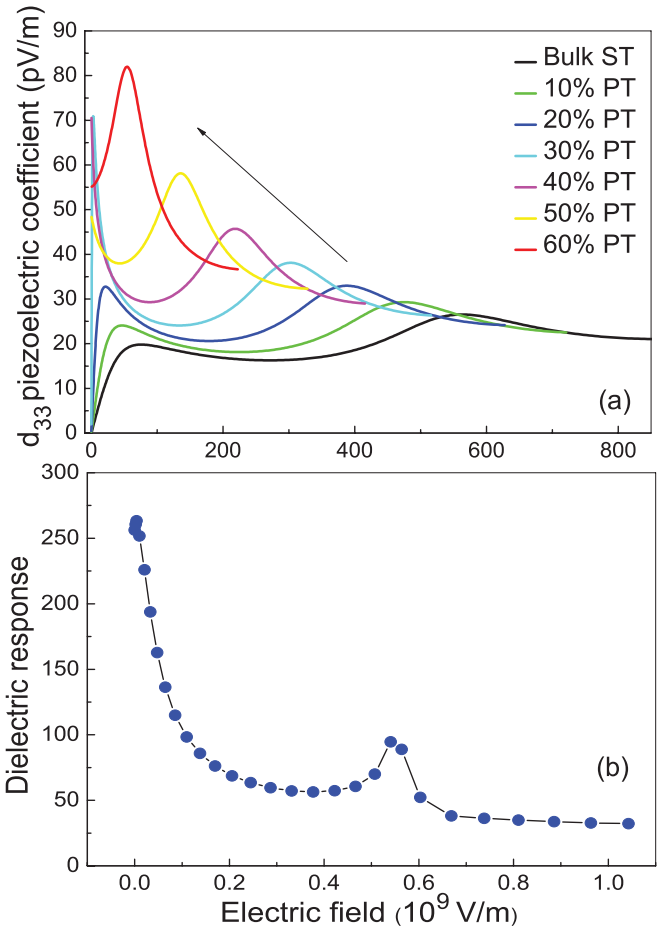


FIG. 3. (Color online) (a) Dependence of $d_{33}(\mathcal{E})$ piezoelectric coefficient on PTO fraction in the $n$PT/$m$ST SL's. (b) Dielectric response of bulk STO as a function of applied electric field, calculated directly from DFT results.

which is responsible for the anomaly observed in the $d_{33}(\mathcal{E})$ coefficient.

Under the fixed-$D$ field, both the FE and AFD ordering is short-ranged. So it should be understood that the $D$ field is the fundamental variable that drives the phase transition at which the threshold $D$ field is reached. Keeping the above concept in mind, we propose that the $D$ field can be increased by a highly polarizable PT component in the PT/ST SL's. As a result of the modified energetics of AFD and FE, the above phase transition, as well as the piezoelectric anomaly, can be observed at a much lower electric field. We then use our developed model to test the above idea. We set up an $n$PT/$m$ST SL, where $n + m = 200$, and we gradually increase the PT fraction from ST bulk $n = 0$. It should be noticed that the interface effect is small in this thick superlattice and can be neglected. The model prediction of the piezoelectric coefficient is presented in Fig. 3(a). As expected, we can see that the SL's become more polarized as the PT fraction is increased. The SL starts from a PE state and becomes FE after the PT fraction in the SL becomes larger than ~30%. As a result of increased FE ordering, the piezoelectric coefficient is generally increased with the anomalous increase corresponding to the phase transition in the ST component. Furthermore, the center of this anomaly is gradually shifted to lower electric field (centered at 55 mV/m for 60% PT fraction). In having increased polarizability from a higher PT fraction in the SL's, the width of the piezoelectric anomaly also becomes smaller, indicating the greatly increased tunability of the applied electric field.

In order to elucidate the physical nature of the peak in both piezoelectric and dielectric response, we expand the internal energy as a function of displacement field $D$ and angle of oxygen octahedral rotation $\varphi$ in the vicinity of the phase transition. The resulting effective Hamiltonian can be written as

$$U_< = U_0 + \alpha D^2 + \beta D^4 + a\varphi^2 + b\varphi^4 - \gamma\varphi^2 D^2, \quad (2)$$

$$U_> = U_0 + \alpha D^2 + \beta D^4. \quad (3)$$

In the above, $U_<$ and $U_>$ denote the energy below and above the phase transition, respectively. $\gamma$ introduces the coupling between AFD and FE and is positive, indicating the competing nature of the two modes. Below the phase transition where AFD and FE coexist, the energy minimum requires that $\partial U/\partial\varphi = 0$, which leads to

$$\varphi^2 = \frac{1}{2b}(\gamma D^2 - a). \quad (4)$$

It can be seen that $\varphi = 0$ above the phase transition [$(\gamma D^2 - a) < 0$] and $\varphi > 0$ below the phase transition [$(\gamma D^2 - a) > 0$], respectively, which is consistent with our computational results. By using Eq. (4), $U_<$ can be reformulated as

$$U_< = U_0 + \alpha D^2 + \beta D^4 + \frac{1}{4b}(\gamma D^2 - a)^2. \quad (5)$$

It is easy to see that $U$ and $\partial U/\partial D = (\Omega/4\pi)\mathcal{E}$ are continuous during the phase transition, where $\Omega$ is the volume of the superlattice. However, $\partial^2 U/\partial D^2 = (\Omega/4\pi)\epsilon^{-1}$ is discontinuous, where $\epsilon_>^{-1} - \epsilon_<^{-1} = 2a\gamma/b$. This is exactly what we see in Fig. 3(b). Thus we can see that the additional peak in $d_{33}(\mathcal{E})$ originates from the discontinuous dielectric constant during the phase transition.

### B. Piezoelectricity at interfaces

AFD and FE competition at interfaces is also found to be of critical importance for its functional properties.[2,4] Here, focusing on the piezoelectricity, we can use our model to study the interface effect in both BT/CT and PT/ST systems. To the above end, we set up the SL model of $n$PT/$n$ST and $n$BT/$n$CT and gradually increase $n$ from the dense interface limit ($n = 1$) to the interface-free limit ($n = \infty$, and here we neglect the possible formation of a nanodomain[24] and free charge on the interfaces). The model prediction of the $d_{33}(\mathcal{E})$ is presented in Fig. 4 [the predicted spontaneous polarizations $P_s$ as a function of $n$ are also plotted in the insets of Figs. 4(a) and 4(b)]. Also given for comparison to our model results in Fig. 4 are the $d_{33}(\mathcal{E})$ calculated directly from our first-principles results. One can see that our model is very accurate in reproducing the first-principles results. In both systems, the SL will have the largest $P_s$ at the dense interface limit ($P_s = 0.187$ C/m$^2$ for 1BT1CT and 0.327 C/m$^2$ for 1PT1ST). The $P_s$ will decrease monotonically until it saturates at 0.21 and 0.14 C/m$^2$ for $n$PT/$n$ST and $n$BT/$n$CT in the interface-free limit. This is consistent with the interface enhancement of polarization found in these materials. Surprisingly, we see also an interface-enhanced piezoelectricity in $n$BT/$n$CT, where $d_{33}(\mathcal{E})$ gains its maximum magnitude at $n = 1$. In contrast, the

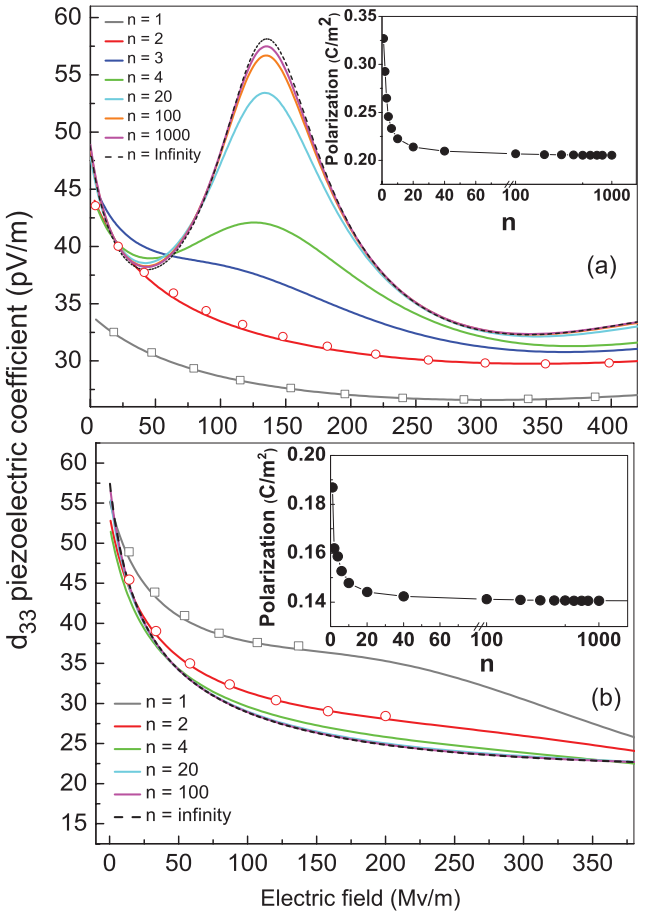


FIG. 4. (Color online) Dependence of $d_{33}(\mathcal{E})$ piezoelectric coefficient on the density of interfaces (symbols represent direct DFT results) in (a) $n$PT/$n$ST SL's and (b) $n$BT/$n$CT SL's.

$n$PT/$n$ST SL's show the opposite effect, where the nonlinear effect corresponding to the ST phase transition starts to be observed when $n = 3$.

The increased $d_{33}(\mathcal{E})$ indicates the structural softening introduced by the interfaces. In FE materials, the structural softening can be found when the system is approaching the FE/PE phase boundary, e.g., with changing in-plane epitaxial strain.[8] As a result, the dielectric and piezoelectric responses diverge in the vicinity of the phase boundary. Strikingly, in BT/CT SL's, the polarization and piezoelectric response can both be increased by the interface, which is crucial for SL design for multifunctional properties.

## IV. CONCLUSION

In summary, we have developed an accurate model that can predict the piezoelectric coefficient of an arbitrary sequence of SL's using the first-principles results of short-period SL's only. The predictive power of the model has been demonstrated in the PT/ST and BT/CT systems, in which AFD and FE are in strong competition. Functional piezoelectricity can be designed in the PT/ST and BT/CT SL's under an applied electric field or a function of the interface density.

## ACKNOWLEDGMENTS

We want to thank M. Stengel for the support of the LAUTREC code package and suggestions on an effective Hamiltonian model. X.W. thanks A. M. Rappe, D. Vanderbilt, and K. M. Rabe for useful discussions. X.W. acknowledges the computational support by the National Science Foundation through TeraGrid resources provided by NICS under Grant No. [TG-DMR100121].

*xifanwu@temple.edu

[1] H. N. Lee *et al.*, Nature (London) **433**, 395 (2005).
[2] E. Bousquet *et al.*, Nature (London) **452**, 732 (2008).
[3] E. Bousquet, J. Junquera, and P. Ghosez, Phys. Rev. B **82**, 045426 (2010).
[4] X. Wu, K. M. Rabe, and D. Vanderbilt, Phys. Rev. B **83**, 020104 (2011).
[5] S. H. Shah, P. D. Bristowe, A. M. Kolpak, and A. M. Rappe, J. Mater. Sci. **43**, 3750 (2008).
[6] J. Y. Jo, R. J. Sichel, H. N. Lee, S. M. Nakhmanson, E. M. Dufresne, and P. G. Evans, Phys. Rev. Lett. **104**, 207601 (2010).
[7] A. Grigoriev, R. Sichel, H. N. Lee, E. C. Landahl, B. Adams, E. M. Dufresne, and P. G. Evans, Phys. Rev. Lett. **100**, 027604 (2008).
[8] C. J. Fennie and K. M. Rabe, Phys. Rev. Lett. **97**, 267602 (2006).
[9] J. Lee *et al.*, Nature (London) **466**, 954 (2010).
[10] J. H. Lee and K. M. Rabe, Phys. Rev. Lett. **104**, 207204 (2010).
[11] J. M. Rondinelli and N. A. Spaldin, Adv. Mater. **23**, 3363 (2011).
[12] S. Seo and H. N. Lee, Appl. Phys. Lett. **94**, 232904 (2009).
[13] X. Wu, M. Stengel, K. M. Rabe, and D. Vanderbilt, Phys. Rev. Lett. **101**, 087601 (2008).
[14] N. Marzari and D. Vanderbilt, Phys. Rev. B **56**, 12847 (1997).
[15] F. Giustino, P. Umari, and A. Pasquarello, Phys. Rev. Lett. **91**, 267601 (2003).
[16] X. Wu, O. Diéguez, K. M. Rabe, and D. Vanderbilt, Phys. Rev. Lett. **97**, 107602 (2006).
[17] S. Seo *et al.*, Adv. Mater. **19**, 2460 (2007).
[18] M. Dawber, N. Stucki, C. Lichtensteiger, S. Gariglio, P. Ghosez, and J.-M. Triscone, Adv. Mater. **19**, 4153 (2007).
[19] P. Aguado-Puente, P. García-Fernández, and J. Junquera, Phys. Rev. Lett. **107**, 217601 (2011).
[20] C. Ederer and N. A. Spaldin, Phys. Rev. Lett. **95**, 257601 (2005).
[21] X. Wu, D. Vanderbilt, and D. R. Hamann, Phys. Rev. B **72**, 035105 (2005).
[22] H. Fu and R. E. Cohen, Nature (London) **403**, 281 (2000).
[23] V. R. Cooper and K. M. Rabe, Phys. Rev. B **79**, 180101 (2009).
[24] P. Zubko, N. Stucki, C. Lichtensteiger, and J.-M. Triscone, Phys. Rev. Lett. **104**, 187601 (2010).
[25] M. Stengel, N. A. Spaldin, and D. Vanderbilt, Nat. Phys. **5**, 304 (2009); M. Stengel, D. Vanderbilt, and N. A. Spaldin, Nature Mater. **8**, 392 (2009); Phys. Rev. B **80**, 224110 (2009).
[26] J. P. Perdew and Y. Wang, Phys. Rev. B **45**, 13244 (1992).
[27] P. E. Blöchl, Phys. Rev. B **50**, 17953 (1994).
[28] The height $h_j$ of layer $j$ is defined as $(\bar{Z}_{j+1} - \bar{Z}_{j-1})/2$, where $\bar{Z}_j$ is the average [001] coordinate of all ions belonging to layer $j$.
[29] See Supplemental Material at http://link.aps.org/supplemental/10.1103/PhysRevB.85.054102 for a breakdown of the rms errors for each of the SL's.
[30] W. Zhong, D. Vanderbilt, and K. M. Rabe, Phys. Rev. Lett. **73**, 1861 (1994).
[31] S. Bhattacharjee, E. Bousquet, and P. Ghosez, Phys. Rev. Lett. **102**, 117602 (2009).
[32] N. Sai and D. Vanderbilt, Phys. Rev. B **62**, 13942 (2000).
[33] E. Courtens, Phys. Rev. Lett. **29**, 1380 (1972).